ChemSusChem

Research Article
doi.org/10.1002/cssc.202300818

Chemistry Europe
European Chemical Societies Publishing

www.chemsuschem.org

Silver Supported Nanoparticles on [Mg_4Al-LDH] as an Efficient Catalyst for the α-Alkylation of Nitriles, Oxindoles and Other Carboxylic Acid Derivatives with Alcohols

Luis Izquierdo-Aranda,[a] Rosa Adam,*[a, b] and Jose R. Cabrero-Antonino*[a]

An efficient heterogeneous silver-catalyzed α-alkylation of nitriles and oxindoles using alcohols via borrowing hydrogen strategy has been developed for the first time. The active nanostructured material, namely [Ag/Mg_4Al-LDH], composed by silver nanoparticles (3-4 nm average particle size) homogeneously stabilized onto a [Mg_4Al-LDH] support with suitable Brønsted basic properties, constitutes a stable catalyst for the sustainable building of novel C–C bonds from alcohols and C-nucleophiles. By applying this catalyst, a broad range of α-functionalized nitriles and oxindoles has been accessed with good to excellent isolated yields and without the addition of external bases. Moreover, the novel silver nanocatalyst has also demonstrated its successful application to the cyclization of *N*-[2-(hydroxymethyl)phenyl]-2-phenylacetamides to afford 3-arylquinolin-2(1*H*)-ones, through a one-pot dehydrogenation and intramolecular α-alkylation. Control experiments, kinetic studies, and characterization data of a variety of [Ag/LDH]-type materials confirmed the silver role in the dehydrogenation and hydrogenation steps, while [Mg_4Al-LDH] matrix is able to catalyze condensation. Interestingly, these studies suggest as key point for the successful activity of [Ag/Mg_4Al-LDH], in comparison with other [Ag/LDH]-type nanocatalysts, the suitable acid-base properties of this material.

Introduction

The design of multifunctional nanomaterials containing catalytic sites with the suitable structural features to mediate a specific chemical transformation is the main goal of heterogeneous catalysis applied to sustainable synthetic chemistry.[1] Obviously, the development of atom-efficient processes starting from available reagents is also a highly relevant issue in modern organic chemistry. The building of new C–C bonds is among the most important transformations in organic chemistry. In the last years, processes such as metal-catalyzed borrowing of hydrogen (BH), also known as hydrogen autotransfer, in which an alcohol is employed as electrophile have been investigated and applied to build novel C–C bonds.[2] Advantageously, in these reactions, water is the only by-product formed and the use of toxic alkylating agents, such as alkyl halides, is avoided. BH reaction involves a first step of metal-catalyzed dehydrogenation of the corresponding alcohol to afford a carbonyl compound and a metal hydride. Then, in the case of C–C bond formation reaction, the carbonyl compound can undergo condensation with the α-C–H position of another carbonyl compound, nitrile or carboxylic acid derivative to afford an olefin, commonly through the formation of a carbanion type intermediate. Finally, the hydrogen addition from the previously formed metal hydride to the olefin affords the product with the novel C–C bond. From this mechanistic pathway it is possible to deduce that the ideal catalytic system for building new C–C bonds through this strategy needs to include a metal species able to perform dehydrogenation/hydrogenation, as well as a base strong enough to generate the corresponding carbonucleophile.[2c] Hence, designing heterogeneous catalysts including both active centers in their structure is an interesting goal.

Among the materials with basic properties, in the last years layered double hydroxides (LDHs) have received a special attention due to their various applications in different fields (catalysis, polymer science, drug delivery, etc.).[3] LDHs are a class of laminated 2D materials with brucite [$Mg(OH)_2$]-like layers, in which some divalent cations have been replaced by trivalent ones.[3a–d,g,h,4] Hence, these nanostructured solids present positively charged sheets, whose charge is balanced by the presence of anions in the hydrated interlayer. A general formula of $[M^{2+}_{1-x}M^{3+}_x(OH)_2]^{x+}(A^{n-})_{x/n}\cdot yH_2O$, can be defined for LDHs where M^{2+} and M^{3+} constitute the divalent and trivalent cations, with a similar ionic radii, and A^{n-} is the charge-balance interlayer anion. Commonly, while M^{2+}=Mg^{2+}, but also Zn^{2+} or Ca^{2+}, and M^{3+}=Al^{3+}, A^{n-} can be either an anion of inorganic or

[a] L. Izquierdo-Aranda, Dr. R. Adam, Dr. J. R. Cabrero-Antonino
Instituto de Tecnología Química
Universitat Politécnica de València-Consejo Superior Investigaciones Científicas (UPV-CSIC)
Avda. de los Naranjos s/n, 46022, València (Spain)
E-mail: jcabrero@itq.upv.es

[b] Dr. R. Adam
Departament de Química Orgànica, Facultat de Farmàcia
Universitat de València
Av. Vicent Andrés Estellés s/n, 46100, Burjassot, València (Spain)
E-mail: rosa.adam@uv.es

Supporting information for this article is available on the WWW under https://doi.org/10.1002/cssc.202300818

organic nature, being CO_3^{2-}, NO_3^-, or OH^- the most usual ones. As a typical example, commercial hydrotalcite (HT) with the formula $[Mg_6Al_2(OH)_{16}CO_3 \cdot 4H_2O]$ is composed of Mg^{2+}, Al^{3+} cations and carbonate anions in the interlayer space along with water molecules. Structurally, each Mg^{2+} is coordinated with six different OH^- groups in an octahedral distribution and shares edges with neighboring Mg^{2+} or Al^{3+} atoms to create 2D sheets. The presence of such hydroxide layers, as well as the intercalating anions, confers LDHs surface with special Brønsted basic features.

Interestingly, due to the intrinsically architectural properties of LDHs, their surface basicity can be finely modulated either by modification of the molar ratio composition (M^{2+}/M^{3+}) and/or the nature of M^{2+}, M^{3+} and the exchangeable interlayer anion (A^{n-}).[3h,4a] Furthermore, through the well-known memory effect,[4a] a controlled thermal treatment of LDHs at $T > 450\,^{\circ}C$ produces the corresponding derived mixed metal oxides, with Lewis basic character, which can be rehydrated with an alkaline solution affording an LDHs with enhanced Brønsted basic properties. Remarkably, catalytic basic centers in LDHs modulated through all these ways have enabled the synthesis of these materials with a broad range of basicity characters.

Therefore, in the last years this class of Brønsted basic solids has received a remarkable attention due to its interesting applications as basic matrices for stabilizing metal-grafted cations or metal nanoparticles or nanoclusters.[3f,h] Following this strategy, nanostructured heterogeneous systems with good catalytic performances in a wide range of organic transformations have been designed. Moreover, in comparison with common inorganic alkali bases, LDHs can be normally reused, and hence, are more convenient from a sustainable perspective and for industrial purposes.

α-Alkylated nitriles are relevant intermediates in the synthesis of amides, carboxylic acids and ketones.[5] These compounds constitute valuable scaffolds with wide applications in pharmaceutical and fine-chemistry industries.[6] In addition, oxindoles and C3-functionalized oxindoles are N-heterocyclic compounds whose structure is found in many biologically active molecules with medicinal applications[7] and natural products.[7d,e,8] Hence, developing sustainable strategies for the α-alkylation of both nitriles ($pk_a \sim 11–25$)[9] and oxindoles ($pk_a \sim 15–25$)[9] is of interest. Traditional procedures involve the use of toxic alkyl halides and stoichiometric amounts of strong inorganic bases. As a consequence, selectivity problems, N- *vs* C-alkylation and/or dialkylation processes, and the generation of substantial amounts of waste are important disadvantages.[10] Recently, catalytic α-alkylation of nitriles and oxindoles using alcohols via BH strategy has been intensively studied as a more environmentally benign strategy.[2c,d,f] However, most of the reported procedures employ non-reusable homogeneous catalysis,[11] involving sophisticated ligands and/or expensive transition metal complexes, frequently in the presence of stoichiometric amounts of strong bases.[12]

As a greener and more convenient alternative, heterogeneous catalysts have been also developed for such relevant transformations, though in a much less extent (Scheme 1). In fact, in the case of the α-alkylation of nitriles with alcohols, only

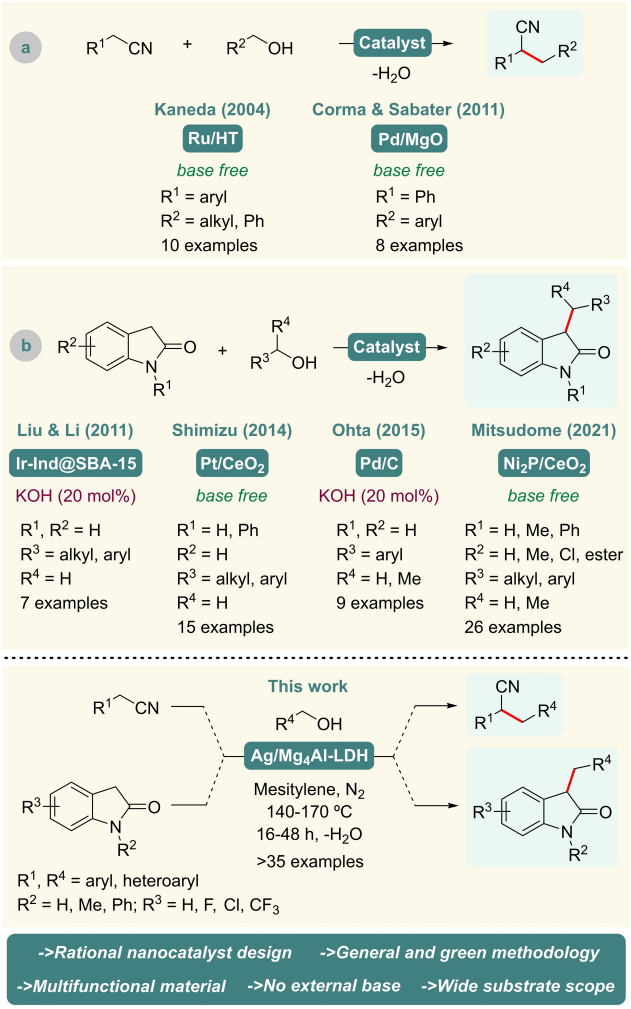

Scheme 1. Top: Heterogeneously catalyzed reported examples for α-alkylation of nitriles (a) or oxindoles (b) using alcohols via borrowing hydrogen methodology. Bottom: [Ag/Mg_4Al-LDH]-catalyzed α-alkylation of nitriles and oxindoles with alcohols reported in this work. HT = hydrotalcite support with a molecular formula $[Mg_6Al_2(OH)_{16}CO_3 \cdot 4H_2O]$. Ind = indene.

two examples have been reported using nanostructured solid materials (Scheme 1a). In 2004, the group of Kaneda developed the first heterogeneous protocol for this reaction.[13] A ruthenium-grafted hydrotalcite, [Ru/HT], was presented as an effective catalyst for this transformation, without needing external bases. However, the necessity of using the alcohol as solvent really hampers its practical application for complex substrates, and a narrow substrate scope was shown. A few years later, Corma and Sabater designed a bifunctional [Pd/MgO] nanomaterial efficient for promoting the α-monoalkylation of phenylacetonitrile, as the only substrate studied, with a small variety of benzyl alcohols at 180 °C.[14] In addition, no isolated yields of the desired α-alkylated nitriles were provided in this case.

A few more examples have been reported for the heterogeneously catalyzed C3 alkylation of oxindoles with alcohols via BH strategy (Scheme 1b).[15] Pioneer examples involved the use of Raney®-nickel in non-catalytic amounts.[16] In general, plati-

num group metals (PGMs) have been involved as active metal centers in such nanostructured catalysts (Ir, Pt or Pd), and in some cases, these systems required the addition of an external base (*i.e.* KOH) to promote enolization.[17] Additionally, substrate scope variation for oxindole moiety was very limited in these examples. Notably, in 2021 the group of Mitsudome developed the only non-noble metal-based heterogeneous protocol for this transformation.[18] Here, a wide range of C3-functionalized oxindoles were accessed with good yields by using a [Ni_2P/CeO_2] material. However, the synthesis of the active nickel-phosphide nanocatalyst needed the use of flammable triphenylphosphite.

In the last years, a few examples of supported silver nanoparticles or nanoclusters on different solid supports have been reported as catalysts in hydrogenation[19] and dehydrogenation[20] processes. Considering these reported activities of Ag supported species, and LDH supports basic properties, we became interested in studying the catalytic application of supported silver nanoaggregates on several LDHs matrices, for the α-alkylation of nitriles and oxindoles with alcohols via BH strategy. Hence, in this work we report the design of a novel silver-based multifunctional nanomaterial, namely [Ag/Mg_4Al-LDH], able to efficiently promote the α-alkylation of nitriles and oxindoles by using alcohols via BH strategy with water as the only byproduct. In addition, this new nanocatalyst is able to mediate for the first time the intramolecular α-alkylation of amides with alcohols to afford 2-quinolinones in a one-pot strategy.

Results and Discussion

With the aim of promoting an effective BH process between an alcohol and a carbonucleophile, such as a nitrile or an oxindole, we started the design of a nanomaterial with multifunctional properties as heterogeneous catalyst. In this direction, we selected LDH materials as suitable supports, with the required Brønsted basic centers able to promote the enolization step,[3h,21] and silver nanoparticles as metal centers with the capacity to mediate dehydrogenation[20] and hydrogenation steps.[19]

As initial point of our study, we prepared different LDH materials via co-precipitation method at controlled pH (see Experimental Section and SI for specific preparation details) composed by Mg^{2+} and Al^{3+} as divalent and trivalent cations, respectively, and with [Mg/Al] molar ratio compositions ranging from 2 to 5 (Mg_2Al-LDH, Mg_3Al-LDH, Mg_4Al-LDH and Mg_5Al-LDH). In addition, two more LDHs either containing Ca^{2+} as the sole divalent cation, [Ca_2Al-LDH], or composed by both Mg^{2+} and Ca^{2+} cations in equimolar combination, [Ca_2Mg_2Al-LDH], were also synthetized for comparison purposes. In all cases, LDHs contained carbonates as interlayer anions, except for [Ca_2Al-LDH] support that contained nitrate to avoid the formation of calcium carbonate. For simplicity reasons, throughout all the discussion the prepared LDHs will be named as [M_xAl-LDH] where M=Mg^{2+}, Ca^{2+} or both, and x = 2, 3, 4 or 5 indicates the molar composition of the divalent cation.

The synthesized materials were characterized by XRPD, thermogravimetric analysis and ^{27}Al MAS NMR (Figure 1, Figure S10 and S11). In addition, their composition was confirmed by inductively coupled plasma-atomic emission spectroscopy (ICP-AES) analysis, together with elemental analysis (Table S8). The XRD patterns of [Mg_xAl-LDH] materials show characteristic (003), (006), (012), (015), (018), (110) and (113) reflections of rhombohedral (3R) LDH structure (Figure 1a).[21c,22] It is interesting to note that LDH materials with higher Mg/Al content present diffraction lines shifted to lower 2θ values, as a consequence of cell expansion caused by higher Mg content.[22e] On the other hand, [Ca_2Al-LDH] presented diffraction peaks at 2θ values fitting with a [Ca_xAl-NO_3-LDH] phase and showing the typical (003), (006) and (110) reflections of LDH phase (Figure 1a).[21c,23] In the case of [Ca_2Mg_2Al-LDH] XRD, (003), (006), (012), (110) and (113) planes characteristic of [MgAl-LDHs] as well as (011), (022), (033) and (014) typical reflections of [CaAl-LDHs] were observed, indicating the formation of a layered structure consisting on both [MgAl-LDH] and [CaAl-LDH] (Figure 1a).[24] Moreover, for all the materials, *d*-spacing could be calculated from the basal 2θ reflection value, (003) plane, and resulted to present a value between 0.76–0.81 nm, corresponding to the thickness of brucite layer plus the intercalated anions and water (Table S7). Lattice parameters *c* and *a* were also determined based on (003) and (110) reflections, respectively, and afforded typical values for these LDH materials (Table S7).[25] Lattice parameter *a*, directly related with cation-cation distance, was significantly higher for [Ca_2Al-LDH] in comparison with [Mg_xAl-LDH] materials, as expected due to the larger ionic radius of Ca^{2+}.[21c]

Thermogravimetric analysis of [Mg_xAl-LDH] materials shows a first weight loss below 227 °C corresponding to interlayer water (Figure S10). A second peak is observed with a maximum between 365–415 °C that can be assigned to the simultaneous dehydroxylation and loss of carbonates.[22c] [Ca_2Al-LDH] presents a very different DTG profile with three clear loss of weights with maximums at 96, 270 and 558 °C that can be interpreted as loss of physisorbed water, interlayer water and a final collapse of the structure by dehydroxylation and loss of nitrates, respectively (Figure S10).[26] Similarly, [Ca_2Mg_2Al-LDH] also displays three loss of weights in its DTG profile centered at 214, 380 and 740 °C (Figure S10).[24b] Finally, the LDH materials were characterized by ^{27}Al MAS NMR and all of them showed a signal at δ ~9–10 ppm corresponding to octahedrally coordinated Al (O_h), confirming the LDH structure (Figure 1c and Figure S11).[21c,22e,27]

Then, the corresponding [Ag/LDH] materials were prepared with a metal charge of 0.5 wt%, determined by ICP-AES. The synthetic methodology implied a wet impregnation of the synthetized LDH supports with an aqueous solution of silver nitrate at 55 °C under darkness, followed by reduction under hydrogen flow at 130 °C during 2 h with a heating ramp of 0.5 °C/min (see Experimental Section and SI for specific details). The integrity of LDH supports was confirmed by XRD and ^{27}Al MAS NMR (Figure 1b and c). Interestingly, XRD patterns of the [Ag/LDH] materials did not show significant changes with respect to LDH supports, suggesting the presence of Ag species of small particle size.

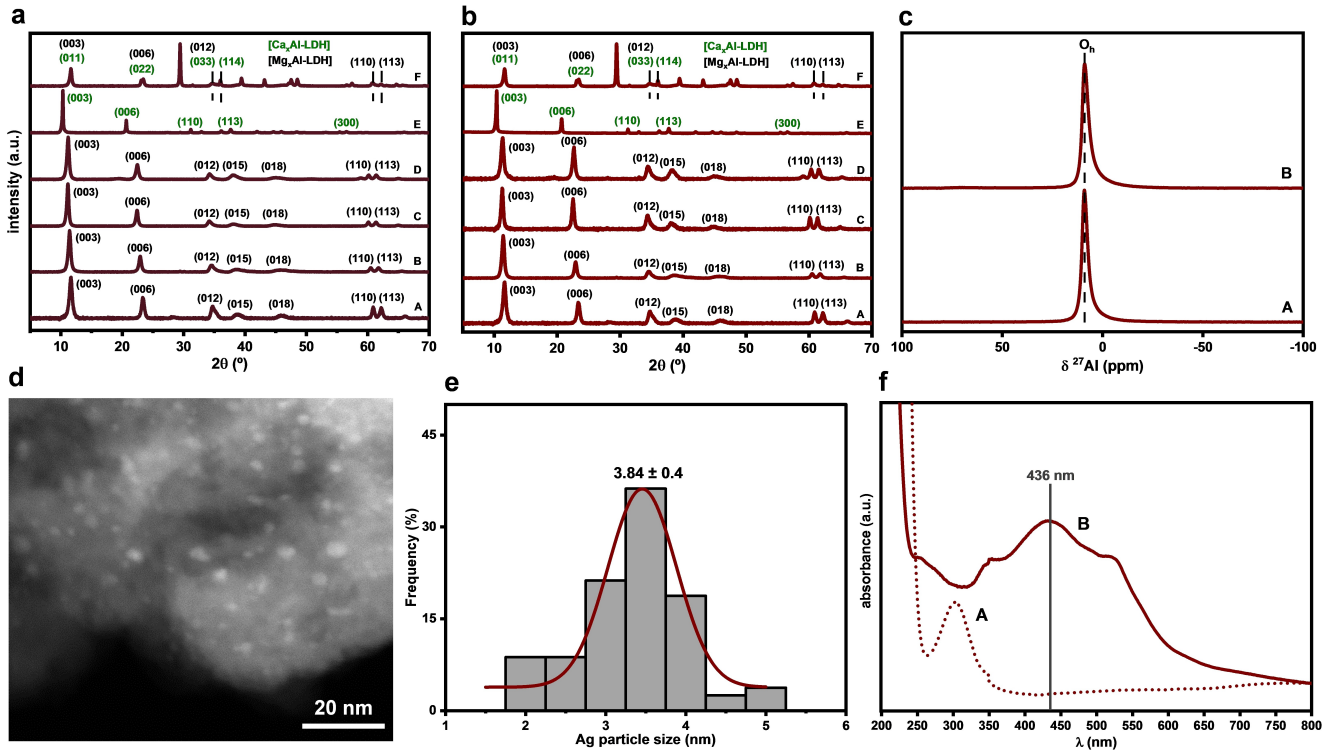

Figure 1. Selected characterization data of [LDH] and [Ag/LDH] nanomaterials: a) XRPD patterns of freshly prepared LDH solid supports: (A) [Mg_2Al-LDH], (B) [Mg_3Al-LDH], (C) [Mg_4Al-LDH]; (D) [Mg_5Al-LDH]; (E) [Ca_2Al-LDH]; (F) [Ca_2Mg_2Al-LDH]; b) XRPD patterns of freshly reduced LDH-supported silver materials at 130 °C and 0.5 °C/min: (A) [Ag/Mg_2Al-LDH], (B) [Ag/Mg_3Al-LDH], (C) [Ag/Mg_4Al-LDH], (D) [Ag/Mg_5Al-LDH], (E) [Ag/Ca_2Al-LDH] and (F) [Ag/Ca_2Mg_2Al-LDH]; c) ^{27}Al MAS NMR spectra of freshly prepared (A) [Mg_4Al-LDH] support and (B) [Ag/Mg_4Al-LDH] material freshly reduced at 130 °C and 0.5 °C/min; d) HAADF-HRSTEM image of freshly reduced [Ag/Mg_4Al-LDH] material at 130 °C and 0.5 °C/min; e) Particle size histogram of the HAADF-HRSTEM study of [Ag/Mg_4Al-LDH] material reduced at 130 °C and 0.5 °C/min; f) Diffuse Reflectance UV-vis spectra of (A) [Mg_4Al-LDH] support, (B) freshly reduced [Ag/Mg_4Al-LDH] material at 130 °C and 0.5 °C/min.

To evaluate the catalytic application of the synthesized nanocatalysts in the selective α-alkylation of nitriles with alcohols via BH, the α-benzylation of phenylacetonitrile **1** with 3 equiv. of benzyl alcohol **2**, was selected as benchmark reaction (Table 1). Firstly, the materials were evaluated using 2.5 mol% of Ag, at 110 °C, employing mesitylene as solvent, during 16 h and under N_2. Interestingly [Ag/Mg_3Al-LDH] material, containing as matrix the well-known hydrotalcite, afforded as products 2,3-diphenylacrylonitrile **3** and 2,3-diphenylpropionitrile **4**, although in low yields of 6% and 8%, respectively (Table 1, entry 1). Then, the other nanomaterials containing different [Mg/Al] molar ratios were evaluated and, to our delight, [Ag/Mg_4Al-LDH] afforded a very high conversion with 7% yield of the unsaturated product **3** and 78% of the desired product **4** (Table 1, entry 3), while low yields were obtained for [Ag/Mg_2Al-LDH] and [Ag/Mg_5Al-LDH] (Table 1, entries 2 and 4). It is relevant to remark that [Ag/Ca_2Al-LDH] and [Ag/Ca_2Mg_2Al-LDH] did not show any activity for the studied reaction (Table 1, entry 5 and 6). These observations clearly demonstrate that the presence of calcium as divalent cation or a Ca/Mg combination in the LDH matrix, results detrimental for the catalytic activity.

At this point, it was interesting to explore other common inorganic supports with diverse range of basicity, such as magnesium spinel ($MgAl_2O_4$), hydroxyapatite (HAP), CeO_2, MgO, γ-Al_2O_3, $Mg(OH)_2$ and $Al(OH)_3$ (Table S1). However, none of these materials resulted active for obtaining the desired product **4**, indicating the great relevance of employing a LDH matrix as a solid support. Indeed, we also decided to explore the effect of the corresponding LDH-derived metal mixed oxide (DO) from [Mg_4Al-LDH] as support of silver nanoparticles, as these materials are known by their characteristic Lewis basicity. With that aim, [Ag/Mg_4Al_1-DO] was prepared by calcination at 450 °C of the parent unreduced [Ag/Mg_4Al-LDH], followed by reduction under H_2 at 130 °C. The formation of the corresponding metal mixed oxide was confirmed by XRD which showed mixed oxide [$MgAlO_x$] typical diffraction peaks as broad signals at 43 and 62° 2θ values (Figure S6).[4a,22e,27a] Nevertheless, this material showed no catalytic activity (Table 1, entry 7) indicating the key role of LDH Brønsted basic sites in this transformation.

Gratifyingly, with a small increase in reaction temperature up to 140 °C, [Ag/Mg_4Al-LDH] nanocatalyst provided much better results affording total conversion of nitrile **1** and a quantitative yield of saturated product **4** (Table 1, entry 8). With this optimum reaction temperature, the influence of additional parameters such as silver catalyst loading, reaction time and amount of alcohol were investigated (Table 1, entries 9–11). In all cases, the use of less catalyst amount (1.5 mol% Ag), shorter reaction times (4 h) or minor excess of **2** (1.5 equiv.) were detrimental for the reaction. Moreover, the solvent effect in the catalytic performance of [Ag/Mg_4Al-LDH] system was also

Table 1. α-Benzylation of phenylacetonitrile **1** with benzyl alcohol **2** catalyzed by supported silver nanocatalysts.

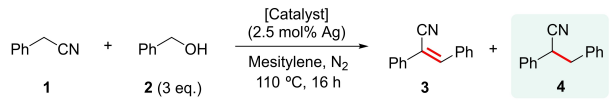

Entry[a]	[Catalyst]	Conv. (%)[b]	**3** (%)[b]	**4** (%)[b]
1	[Ag/Mg_3Al-LDH]	15	6	8
2	[Ag/Mg_2Al-LDH]	14	7	6
3	[Ag/Mg_4Al-LDH]	92	7	78
4	[Ag/Mg_5Al-LDH]	22	7	13
5	[Ag/Ca_2Al-LDH]	–	–	–
6	[Ag/Ca_2Mg_2Al-LDH]	–	–	–
7	[Ag/Mg_4Al-DO]	–	–	–
8[c]	**[Ag/Mg_4Al-LDH]**	**>99**	–	**99**
9[d]	[Ag/Mg_4Al-LDH]	64	19	41
10[e]	[Ag/Mg_4Al-LDH]	71	19	53
11[f]	[Ag/Mg_4Al-LDH]	73	16	48
12[c]	[Mg_4Al-LDH]	<5	3	–
13[c]	–	–	–	–
14[c]	[Ag/*reh*-Mg_4Al-LDH(a)]	60	32	27
15[c]	[Ag/*reh*-Mg_4Al-LDH(b)]	48	27	20
16[g]	[Ag/Mg_4Al-LDH]	54	40	12
17[h]	[Ag/Mg_4Al-LDH]	>99	44	50
18[i]	[Ag/Mg_4Al-LDH] (1th reuse)	>99	2	97
19[i]	[Ag/Mg_4Al-LDH] (2nd reuse)	97	4	92
20[i]	[Ag/Mg_4Al-LDH] (3th reuse)	95	10	85

[a] Standard reaction conditions: phenylacetonitrile **1** (14.5 μL, 0.125 mmol), benzyl alcohol **2** (40 μL, 0.375 mmol, 3 equiv.), freshly reduced solid catalyst (at 130 °C, 2 h, heating ramp of 0.5 °C/min) with a silver content of 0.5 wt% (67 mg, 2.5 mol% Ag), mesitylene (2 mL) at 110 °C under N_2 during 16 h. [b] Conversion of **1** and yields of products **2** and **3** were calculated by GC using hexadecane as internal standard. [c] Run at 140 °C. [d] Run at 140 °C using 40 mg of catalyst (1.5 mol% Ag). [e] Run at 140 °C during 4 h. [f] Run at 140 °C and with 1.5 equiv. of benzyl alcohol **2**. [g] Run at 140 °C under air. [h] Run with non-reduced [Ag/Mg_4Al-LDH] material (67 mg, 2.5 mol% Ag). [i] Consecutive reuses of the catalytic material performed at 140 °C (see SI for a detailed recycling procedure), using a freshly reduced material before each new reaction cycle.

examined (Table S2). Among the different solvents tested, mesitylene gave the best results.

In addition, both silver nanoparticles and LDH support showed to be essential for the catalytic performance of the material. In the absence of silver nanoparticles, only traces of product **3** were detected (Table 1, entry 12). Moreover, no conversion of nitrile **1** was reached performing the reaction without [Ag/Mg_4Al-LDH] material (Table 1, entry 13).

With the aim of further tuning the support properties, we decided to explore the effect of employing a [Mg_4Al-LDH] rehydrated support in the catalytic activity of the final material.[4a,21c,27c,28] Thus, we prepared and tested [Ag/*reh*-Mg_4Al-LDH] system in two different ways. On one hand, method (a) consisted in the impregnation of silver cations using a $AgNO_3$ aqueous solution onto a metal mixed oxide support matrix, previously obtained from calcination of parent [Mg_4Al-LDH] at 450 °C. Due to the well-known memory effect of LDHs, there is a simultaneous impregnation of silver cations and conversion of the derived mixed oxide into LDH. Complementarily, method (b) implied the impregnation of silver cations onto a previously rehydrated LDH support, obtained from calcination of [Mg_4Al-LDH] at 450 °C followed by rehydration with a NaOH 1 M aqueous solution. XRD analysis of both materials confirmed a LDH structure, although with a lower degree of crystallinity in comparison with the standard material (Figure S7).[4a,29] In addition, LDH structural integrity of both samples was also demonstrated by ^{27}Al NMR, since all aluminum cations are disposed in an octahedral (O_h) conformation (Figure S13). Unfortunately, both freshly reduced versions of the material at 130 °C, [Ag/*reh*-Mg_4Al-LDH(a)] and [Ag/*reh*-Mg_4Al-LDH(b)], resulted much less active when compared with [Ag/Mg_4Al-LDH] system (Table 1, entry 14 and 15).

At this point, we became interested in evaluating the catalytic activity of other metal supported nanoparticles onto [Mg_4Al-LDH] matrix. With this aim, different materials composed by Ru, Fe, Co, Ni, Cu, Mn or Bi NPs stabilized on the optimal LDH support were prepared and tested under the previously optimized reaction conditions (Table S3). It should be noted that to ensure a total reduction of the grafted metal cations without varying the original LDH nature of the support, chemical reduction of the materials using an excess of aqueous $NaBH_4$ was applied, instead of reduction under H_2 flow at 130 °C. For comparison purposes, a chemically reduced [Ag/Mg_4Al-LDH] material was also prepared. Among the different metals tested, silver showed a superior activity promoting the formation of the saturated product **4**. Under this reaction conditions, Ru, Fe, Co, Ni, Cu, Mn or Bi metals resulted poorly active affording mainly the α-olefinated compound **3** in moderate to low yields (Table S3). In addition, it was shown that reduction of silver cations employing H_2 flow at 130 °C afforded a more efficient catalyst in comparison with the one obtained by chemical reduction with $NaBH_4$ (Table S3, entries 8 and 9).

In order to better understand [Ag/Mg_4Al-LDH] as catalytic system, the reaction was performed under aerobic conditions (Table 1, entry 16) or under N_2 using the non-reduced material (Table 1, entry 17). Under these conditions, poorer results were achieved, revealing the relevance of both reduction step in the catalyst preparation, as well as the use of anaerobic conditions for promoting an effective alcohol dehydrogenation. Taking into account these results, we became interested in investigating the influence of the reduction ramp employed in the catalyst preparation in the final material. Thus, we obtained the corresponding nanomaterials at heating ramps of 1, 2 and 4 °C/min under H_2 flow and the catalytic activity of these materials was evaluated (Table S4 and Figure S9). From these experiments, we could check that original [Ag/Mg_4Al-LDH] catalyst reduced at 0.5 °C/min, was the most active. Notably, a clear relationship between the material activity and the reduction ramp was observed with the material reduced at 4 °C/min being

the least effective, affording 63% conversion of **1** and 49% yield of the desired product **4** (Table S4, entry 4).

To further optimize the active nanocatalyst, we prepared two additional [Ag/Mg_4Al-LDH] systems with different silver loadings (0.25 and 1.5 wt%). Catalytic evaluation of these materials clearly revealed that the originally selected metal charge (0.5 wt% Ag) resulted as the best choice (Table S5).

To complete the characterization of the [Ag/Mg_xAl-LDH] materials, nitrogen adsorption-desorption isotherms were performed to study the specific surface area and the pore-size distribution (Table S9). Surface areas between 28.7–70.6 m^2/g were determined, in the usual range for this class of materials.[22e,27c] Moreover, [Ag/Mg_4Al-LDH] was examined by high-angle annular dark-field-high-resolution scanning transmission electron microscopy (HAADF-HRSTEM) and energy-dispersive X-ray (EDX) elemental analysis (Figure 1d and e, Figure S18). Through these techniques, it was possible to confirm the presence of Ag nanoparticles in the [Mg_4Al-LDH] support and it could be determined an average particle size of 3.8 nm. X-Ray photoelectron spectroscopic (XPS) study demonstrated the presence of the characteristic Ag 3d doublet with the position of $3d_{5/2}$ peak at 368.4 eV (Figure S16).[19b,30] However, the assignment of the corresponding Ag oxidation state through this technique was not possible due to the difficulty in determining the Auger parameter in such a silver low loaded sample. With the aim of clarifying this point, DR UV-Visible spectroscopy as well as electron paramagnetic resonance (EPR) were employed for further characterization of [Ag/Mg_4Al-LDH] nanocatalyst (Figure 1f and Figure S15). Interestingly, EPR spectra showed an axially symmetric signal with *g* value 2.09, attributed to Ag(0) nanoparticles (Figure S15).[31] In addition, UV-Vis spectrum has been used to identify different Ag species, and the presence of Ag metallic nanoparticles was demonstrated to show a band with a maximum between 400–600 nm.[32] In the case of [Ag/Mg_4Al-LDH], DR UV-Vis spectra showed a maximum of absorption at 436 nm, which can be assigned to metallic Ag species (Figure 1f).

Then, the heterogeneous nature of the optimal [Ag/Mg_4Al-LDH] system was verified by a hot filtration test (see SI, section 6.1 and Figure S5). Moreover, ICP-AES analysis of the reaction mixture and [Ag/Mg_4Al-LDH] nanomaterial after reaction, revealed that no leaching of silver species takes place under the employed reaction conditions (see SI, section 6.2). Thus, reusability studies using a freshly reduced [Ag/Mg_4Al-LDH] system after each cycle were performed and, to our delight, it was found that the nanocatalyst preserves its catalytic efficiency even after four cycles of reaction (Table 1, entries 18–20). [Ag/Mg_4Al-LDH] material after one reaction cycle was examined by HAADF-HRSTEM and an increase in the average Ag particle size to 8.1 nm was measured (Figure S19). In fact, XRD patterns of used [Ag/Mg_4Al-LDH] material, both before and after reduction, showed the (111) plane at 2θ 38.3° corresponding to metallic Ag, as well as the typical reflections of LDH in a broader fashion, indicating the increase in Ag particle size and some loss of crystallinity of the support (Figure S8). XPS study of the material after reaction showed no changes (Figure S17). Interestingly, DR UV-Visible spectra of [Ag/Mg_4Al-LDH] showed a band with a maximum at 409 nm that confirms the presence of Ag metallic species (Figure S14). These results indicate that the catalyst has a considerable but, probably, limited durability. The fact that the catalyst is active even when Ag particle size is increased can be explained if Ag larger nanoparticles are also active until certain point, or if the amount of Ag smaller particles is enough to maintain the activity.

To confirm the BH mechanism and better understand our developed catalytic system, we designed and performed several control experiments and kinetic studies. First, we checked the role of our catalyst in the three main steps of the BH mechanism through a series of control experiments (Scheme S2). It was shown that our [Ag/Mg_4Al-LDH] system was able to catalyze the initial dehydrogenation of benzyl alcohol **2** (Scheme S2a). However, in the absence of a coupling partner, benzaldehyde **5** was obtained in low yields due to its degradation, and an incomplete conversion of **2** was observed. The second step involving a deprotonation to afford a nitrile anion followed by condensation with the aldehyde, was investigated through the reaction between phenylacetonitrile **1** and benzaldehyde **5** at 140 °C. It was demonstrated that this step worked smoothly, even at milder conditions of 110 °C, using as catalysts either [Ag/Mg_4Al-LDH] or [Mg_4Al-LDH] (Scheme S2b and c). Finally, the transfer hydrogenation of 2,3-diphenylacrylonitrile **3** with benzyl alcohol **2** as hydrogen donor to afford 2,3-diphenylpropionitrile **4** was tested employing [Ag/Mg_4Al-LDH] or [Mg_4Al-LDH] as catalysts (Scheme S2d and e). Interestingly, this reaction only worked in the presence of [Ag/Mg_4Al-LDH], totally discarding a base-catalyzed Meerwein-Ponndorf-Verley (MPV) reduction.[33]

Once the BH mechanism was confirmed, as well as the multifunctional character of our catalyst operating in the different steps, we decided to investigate the yield time kinetic profile of the optimized reaction (Figure S1). It is interesting to note that at short reaction times, benzaldehyde **5** was not detected and unsaturated product **3** was the only detected intermediate, although in a maximum yield of 16%. Indeed, an initial rate of 13.0%/h was measured for our global process at 140 °C with [Ag/Mg_4Al-LDH], in contrast with an initial rate of 312.6%/h for the condensation step at 110 °C with the same catalyst (Figure S1 and S2). These data clearly indicate a fast condensation step and, hence, that the rate limiting step is either the dehydrogenation or the hydrogen transfer. In order to elucidate which of these steps is the rate limiting one, kinetic orders of nitrile **1** and alcohol **2** for the α-alkylation of **1** with **2** were investigated (see Figures S3 and S4).[14] Those experiments clearly manifested that, whilst initial reaction rate remains unaltered with variation of nitrile **1** concentration, the value is notably affected by the modification of alcohol **2** concentration. This observation suggests that alcohol dehydrogenation is the rate-limiting step of the mechanism, since it is the only one in which nitrile is not involved.

With the aim of acquiring a deeper knowledge of the catalytic behavior of our [Ag/Mg_4Al-LDH] system *vs* the other [Ag/Mg_xAl-LDH] materials, a kinetic comparison of these materials was performed at the optimized reaction conditions. Initial reaction rates, as well as final yields, of the global process

and the condensation step were investigated for all the materials (Figure 2 and Table S6). It is widely accepted that the number of basic Brønsted sites in [Mg_xAl-LDH] materials increases with the decrease of magnesium content, as this decrease means a larger Al^{3+} content and, hence, a higher amount of balancing anions conferring basicity.[3h,4a,29] Therefore, if the initial rate of a reaction was exclusively dependent on the Brønsted basicity, an increase in reaction efficiency would be expected with a decrease in "x" value.[34] In our case, we observe the opposite effect reaching a maximum of activity for [Ag/Mg_4Al-LDH] system, and then, a significant decrease for [Ag/Mg_5Al-LDH] for both global process and condensation steps (Figure 2 and Table S6). This kind of complex behavior has been observed before in multi-step reactions catalyzed by a combination of acid (M^{2+} or M^{3+}) and basic sites present in LDH materials, such as the cyanoethylation of alcohols.[34] In this case, it has been reported that reaction efficiency depends on a combination of a series of factors such as number of acid and basic sites, strength of these sites and accommodation of intermediate species. In the studied process here of BH between an alcohol **1** and a nitrile **2**, we are also in a complex situation. It is reported that rate limiting step of dehydrogenation, although mainly catalyzed by silver species, is assisted by acid and basic sites of the support.[35] Similarly, hydrogenation can also be influenced by this kind of active sites.[36] On the other hand, the α-deprotonation of nitrile, obviously, needs the assistance of basic sites.[37] In addition, it has also been reported that Lewis acid sites of LDH (Al^{3+} centers) can have an important role coordinating nitrogen of nitrile to increase α-H acidity and enable α-deprotonation.[37] Our results here show that [Ag/Mg_4Al-LDH] system presents the optimal acid-base properties, as well as Ag species, to catalyze both the global process and the condensation (r_0 **4** (%/h) of 13 and r_0 **3** (%/h) > 300) (Figure 2 and Table S6). Remarkably, [Ag/Mg_2Al-LDH] is totally inactive for both reactions, while [Ag/Mg_3Al-LDH] and [Ag/Mg_5Al-LDH] are able to catalyze these processes but in moderate or low yields and initial rates (r_0 **4** (%/h) of 5–10, **4** yield of 35–46% and r_0 **3** (%/h) of 55–48, **3** yield of 37–53%) (Figure 2 and Table S6).

With all these data in hand, we can propose a mechanism entailing the borrowing of hydrogen between nitrile **1** and alcohol **2** (Scheme 2). First, a silver-catalyzed dehydrogenation of benzyl alcohol **2** gradually generates benzaldehyde **5**, as well as silver nanoparticle hydride species. This has been determined as the rate-limiting step of the whole process. Then, a fast condensation between benzaldehyde **5** and nitrile **1** occurs, implying a previous nitrile enolization under the reaction conditions. It is important to remark that the fact that the

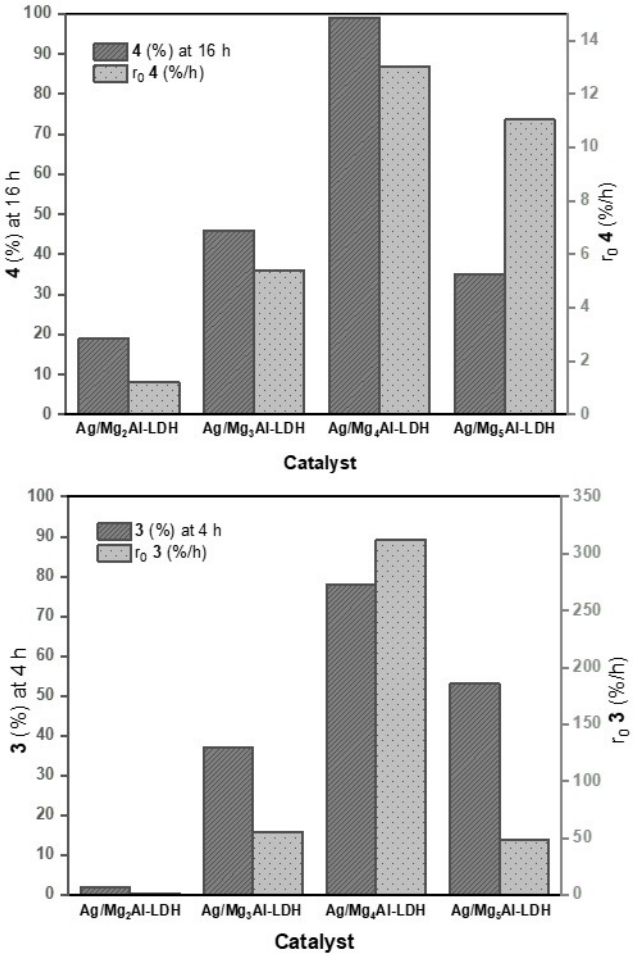

Figure 2. Initial reaction rates of **3** and **4** formation (r_0) expressed as [yield (%)/h] and yield of **3** and **4** at a defined reaction time for (up) α-alkylation of phenylacetonitrile **1** with benzyl alcohol **2** (3 equiv.) at 140 °C and (bottom) condensation step between phenylacetonitrile **1** and benzaldehyde **5** (3 equiv.) at 110 °C in the presence of different [Ag/Mg_xAl-LDH] materials. For detailed reaction conditions, see SI. Yield of products **3** and **4** were calculated by GC using hexadecane as internal standard. Initial rate (r_0) is the slope of the linear equation: [yield of **3** (%) = r_0×t (h)] or [yield of **4** (%) = r_0×t (h)] defined at initial reaction times and expressed as [r_0 **3** (%/h)] or [r_0 **4** (%/h)].

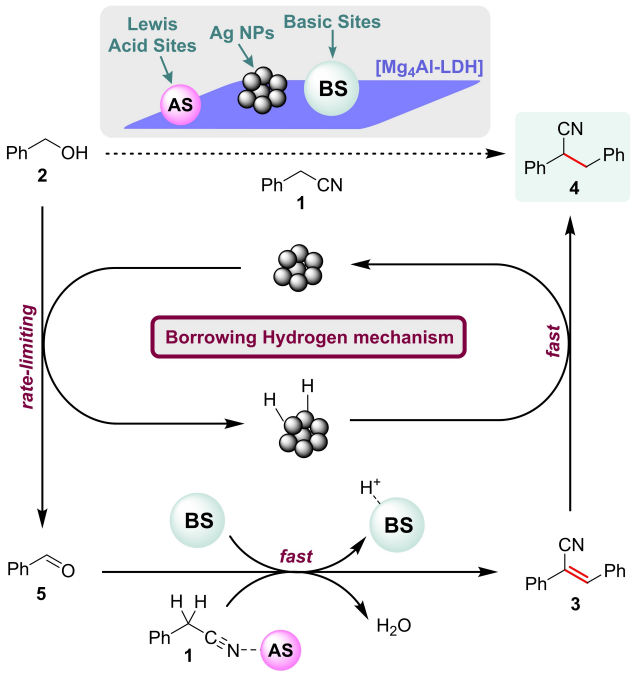

Scheme 2. Plausible reaction mechanism for the α-alkylation of phenylacetonitrile **1** with benzyl alcohol **2** in the presence of [Ag/Mg_4Al-LDH] nanocatalyst.

condensation step undergoes at such high speed, limits the aldehyde degradation. In addition, control experiments showed that condensation step is catalyzed by [Mg_4Al-LDH] basic and acid sites. Finally, it is proposed the reduction of the α,β-unsaturated nitrile **3** catalyzed by surface silver nanoparticle hydride species on the [Mg_4Al-LDH] support to afford the desired α-alkylated nitrile **4**. As it has been commented before, characteristic Brønsted basic sites of [Mg_4Al-LDH], but also Lewis acid sites, are proposed to present a prominent role assisting dehydrogenation, condensation and hydrogenation steps.

Once established the catalytic performance of [Ag/Mg_4Al-LDH] nanomaterial in the α-benzylation of phenylacetonitrile **1** with benzyl alcohol **2**, we decided to investigate its range of application for a variety of nitrile and alcohol substrates (Scheme 3, A). To ensure a total conversion of nitriles and/or an improvement of the final product yield, higher catalyst amounts (5 mol% Ag), larger excess of alcohol (5 equiv.) and/or extended reaction times up to 48 h were applied in some cases.

Apart from 2,3-diphenylpropionitrile **4** obtained in a 97% yield, different α-benzylated arylacetonitriles (**6**–**13**) bearing halogen (F), alkoxy (–OPh, –OEt), alkyl (–*i*Pr, –Me), phenyl or trifluoromethoxy functionalities in *ortho*-, *meta*- and/or *para*-position could be accessed in good to excellent isolated yields (70–90%) by coupling the parent aryl-substituted nitrile with benzyl alcohol **2**. In addition, 2-naphthaleneacetonitrile, 1,3-benzodioxole-5-acetonitrile as well as pyridine- and thiophene-containing acetonitriles, in combination with **2**, afforded the desired nitrile products (**14**–**17**) with notable yields (76–95%). Interestingly, under the selected optimized reaction conditions, α-olefinated nitrile **17** could be isolated as the sole product in this case.

Additionally, when phenylacetonitrile **1** was reacted with several *meta*- and/or *para*-substituted benzyl alcohols with methoxy, nitro, chloro, methylthio or methyl groups, the desired functionalized nitriles (**18**–**22**) were obtained in excellent yields (78–94%). It should be noted that in the case of 3-nitrobenzyl alcohol, α-olefinated nitrile **19** was obtained as the final product. To our delight, the present protocol was also successfully applicable to *N*-heterocycle containing alcohols such as 4-pyridinemethanol or 6-quinolinemethanol affording the corresponding α-functionalized nitriles **23** and **24** in 70 and 80% yield, respectively.

Gratifyingly, the designed silver nanocatalyst also resulted highly effective for promoting α-functionalizations of a wide range of 2-oxindoles with several alcohols via BH under previously employed reaction conditions (Scheme 3, B). Interestingly, although free NH position in oxindoles is also prone to alkylation, the nanostructured catalyst exhibited total selectivity towards C3-functionalization. By applying this methodology, highly diverse α-functionalized 2-oxindoles could be obtained after purification. Notably, in addition to simple 2-oxindole, several oxindole derivatives functionalized with halogens (F and Cl) or a trifluoromethyl group at 5-, 6- or 7-position were successfully coupled with alcohol **2**, affording the desired α-benzylated oxindoles (**25**–**30**) with good or excellent isolated yields (74–94%). Unfortunately, 2-oxindoles 5-substituted with electron-donating groups, such as methoxy or amino, did not afford the desired product in good yields, affording poor selectivities or only traces of the product, respectively. In addition, not only NH-free oxindoles, but also *N*-methyl or *N*-phenyl substituted derivatives were converted to the desired C3-benzylated products (**31** and **32**) in an efficient manner (84 and 94% yield, respectively). Moreover, even more structurally complex oxindoles were accessed successfully by crossing several 2-oxindole counterparts with a variety of substituted benzylic alcohols. Remarkably, benzyl alcohols substituted with methylthio, methoxy, chloro, methyl and trifluoromethoxy groups in *meta*- and/or *para*- positions, as well as heterocycle-containing alcohol derivatives could be employed for obtaining the target C3-functionalized oxindole products (**33**–**40**) with good yields (71–90%). This type of valuable organic compounds constitutes a potential class of biologically active molecules with interesting applications.

In comparison with α-alkylation of acetonitriles or oxindoles, the use of more deactivated carboxylic acid derivatives, such as simple amides, is significantly hampered owing to their very low α-carbon acidity (pK_a~30–35).[9] Despite this difficulty, this transformation has been recently investigated employing sophisticated homogeneous catalysts in the presence of excess of strong bases (*i.e.* KO*t*-Bu).[38] To the best of our knowledge, in the heterogeneous area only one example has been reported in 2022 by Obora's group.[39] In this work, unsupported ruthenium nanoparticles stabilized on very specific conditions and in combination with (over)stoichiometric amounts of a strong base, are capable to promote α-alkylation of unactivated amides with alcohols. Hence, there is a high interest in the design of a solid, stable and reusable nanostructured catalyst combining basic sites capable to promote the enolization at the C_α of the amide, and metal species able to mediate dehydrogenation and hydrogenation steps.

To our delight, the novel [Ag/Mg_4Al-LDH] nanomaterial is also able to mediate the intramolecular α-alkylation of slightly α-activated amide groups with primary alcohols, affording 3-arylquinolin-2(1*H*)-ones in one-pot (Scheme 4). This kind of *N*-heterocycles are considered privileged scaffolds in therapeutic and medicinal chemistry, with widespread applications.[40] Traditional organic approaches to access them are based on Friedlander,[41] Knorr[42] or Vilsmeier-Haack[43] protocols working through the condensation between an amide and a carbonyl function. In addition, modern strategies involving homogeneously metal-catalyzed processes have been developed for their synthesis.[40c,44] Considering the high interest of these compounds, the development of alternative and more sustainable methodologies for obtaining them is a sought as a relevant goal nowadays in organic chemistry and catalysis.

With the aim of evaluating our developed catalytic system in a dehydrogenative strategy to obtain 3-arylquinolones, different *N*-[2-(hydroxymethyl)phenyl]-2-phenylacetamides (**S1**–**S5**) were prepared as starting materials. These compounds were obtained via the selective *N*-acylation process of the corresponding 2-aminobenzyl alcohols (see SI for experimental details).[45] Interestingly, when our [Ag/Mg_4Al-LDH] catalytic system was studied for the aimed reaction, it was found that the best results were obtained when the reaction was run first

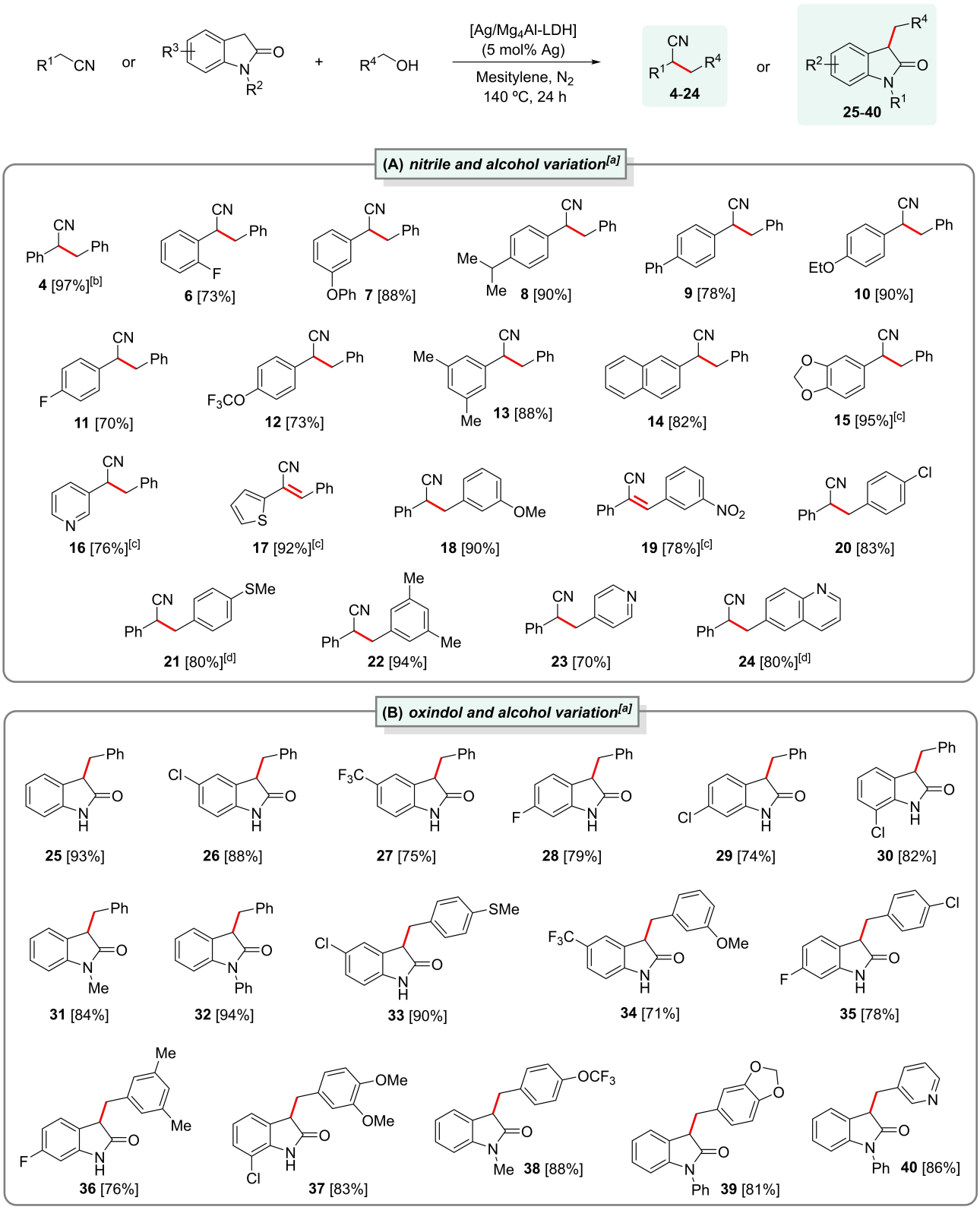

Scheme 3. Synthesis of α-functionalized (A) nitriles and (B) 2-oxindoles through [Ag/Mg_4Al-LDH]-catalyzed α-alkylations using primary alcohols via BH strategy. [a] Standard reaction conditions: nitrile or oxindole (0.125 mmol), alcohol (0.375 mmol, 3 equiv.), freshly reduced [Ag/Mg_4Al-LDH] catalyst (at 130 °C, 2 h, heating ramp of 0.5 °C/min) with a silver content of 0.5 wt% (134 mg, 5 mol% Ag), mesitylene (1.5 mL) at 140 °C under N_2 during 24 h. Yields of isolated products are given between brackets. [b] Run with 2.5 mol% Ag (67 mg of catalyst). [c] Run with alcohol (0.625 mmol, 5 equiv.) for 48 h. [d] Run during 48 h.

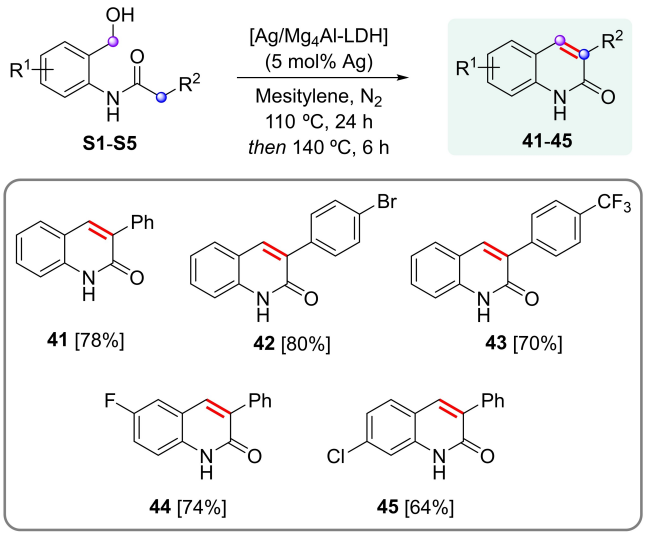

Scheme 4. [Ag/Mg_4Al-LDH]-catalyzed one-pot synthesis of 3-arylquinolin-2(1*H*)-ones **41**–**45** from the intramolecular α-alkylation of 2-phenylacetamide groups with primary alcohols. Standard reaction conditions: *N*-[2-(hydroxymethyl)phenyl]-2-phenylacetamide **S1**–**S5** (0.125 mmol), freshly reduced [Ag/Mg_4Al-LDH] catalyst with a silver content of 0.5 wt% (134 mg, 5 mol% Ag), mesitylene (2 mL), under N_2 at 110 °C during 24 h and then at 140 °C over 6 h. Yields of isolated products are given between brackets.

at 110 °C during 24 h, to afford the intermediate aldehyde, and then at 140 °C over 6 h, to promote enolization/cyclization. Employing these specific conditions, it was avoided reagent degradation and final product yield was improved. Gratifyingly, by applying this original strategy, several 3-aryl substituted 2-quinolinones (**41**–**45**) were accessed with moderate to good yields (64–80%, Scheme 4). Remarkably, halogen atoms such as F, Cl and even Br were fully tolerated as well as the relevant trifluoromethyl group affording the desired *N*-heterocycles in an efficient manner. It should be mentioned that in this case BH mechanism was not completely closed, since final hydrogen transfer does not occur,[46] probably because of the difficulty of reducing an internal double bond in a 2-quinolinone fragment.

Conclusions

We have designed [Ag/Mg_4Al-LDH] material as a reusable and efficient nanocatalyst for the α-alkylation of a wide range of nitriles and 2-oxindoles using alcohols via BH strategy. Detailed characterization of the active material was performed (ICP-AES, XRPD, TG, BET Area, ^{27}Al MAS NMR, XPS, HAADF-HRSTEM, DR UV-Vis and EPR) revealing its constitution by small silver nanoaggregates (3.8 nm of average particle size) homogeneously distributed across a LDH support with a [Mg/Al] molar ratio of 4. Kinetic and mechanistic investigations of a series of [Ag/Mg_xAl-LDH] (x = 2, 3, 4 and 5) materials as catalysts in this reaction demonstrated that [Ag/Mg_4Al-LDH] material, presenting a moderate basicity, is the most active catalyst for both dehydrogenation and condensation steps. In addition, the borrowing hydrogen mechanism was confirmed for explaining this process. Moreover, the strategy has been widened to the challenging α-CH activation of amides, and quinolin-2(1*H*)-ones could be obtained via a one-pot intramolecular cyclization of *N*-(2-(hydroxymethyl)phenyl)-2-phenylacetamides. Thus, for the first time, this kind of *N*-heterocycles with many applications has been obtained through this dehydrogenative protocol with the developed [Ag/Mg_4Al-LDH] system. Interestingly, the results presented herein could open the door to the development of novel and sustainable methodologies towards the synthesis of valuable organic compounds from accessible and stable starting materials employing heterogeneous nanocatalysts.

Experimental Section

General information. Mg-, Ca- and Al-based LDH supports, reduced catalysts and non-reduced material versions (if indicated) were analyzed by X-ray powder diffraction (XRPD) using a Cubix-Pro PANalytical diffractometer equipped with a detector PANalytical X'Celerator (CuK_α radiation). The wt% amount of Mg, Ca and Al present in the synthesized LDHs, the wt% amount of Ag, Ru, Fe, Co, Ni, Cu, Mn or Bi contained in the freshly reduced metal catalysts and the wt% amount of silver present in the used [Ag/Mg_4Al-LDH] catalyst, were determined by inductively coupled plasma-atomic emission spectrometer (ICP-AES) using a Varian 715-ES after the dissolution of the solid samples in HNO_3:HCl aqueous solution (1:3 vol). The wt% amount of carbon and nitrogen present in the Mg-, Ca- and Al-based LDH solids was determined by elemental analysis using a EURO EA elemental analysis equipment (Eurovector) coupled with a TCD. Liquid nitrogen adsorption of the selected LDH-based materials was analyzed using N_2 adsorption isotherms at −196 °C in a Micrometrics FlowSorb equipment. The specifics surface areas of the selected samples were calculated by applying the Brunauer-Emmett-Teller (BET) model over the rage P/P^0 = 0.05–0.25 of the isotherms and the average pore diameter was calculated by applying the Barrett-Joiner-Halenda (BJH) desorption model. Freshly reduced [Ag/Mg_4Al-LDH] catalyst and used catalyst were observed by HRSTEM and HRTEM by using a JOEL JEM 2100F electron microscope working at 200 kV. The gravimetric analysis during the thermal decomposition of the Mg-, Ca- and Al-based LDH supports was studied from room temperature to 900 °C, at a heating rate of 10 °C min^{-1}, under air flow using a Netzsch STA 449 F3 Jupiter thermal analyzer. The analysis was performed employing approximately 10 mg of the sample on a crucible of aluminium oxide. Diffuse reflectance UV-Vis spectra of the selected samples were obtained on a Cary 7000 (Agilent Technology) instrument equipped with a Harrick "Praying Mantis" cell, using $BaSO_4$ as a reference for reflectance. Electron paramagnetic resonance (EPR) analysis of the reduced [Ag/Mg_4Al-LDH] catalyst was performed in a Bruker EMX-12 instrument operating in X band at 9.5 GHz, modulation amplitude of 1 G and modulation frequency of 100 KHz. ^{27}Al magic angle spinning nuclear magnetic resonance (MAS NMR) spectra of selected LDH-based supports and materials were recorded at room temperature with a Bruker AV III HD 400 spectrometer at 104.6 MHz using a 3.2 mm probe spinning the samples at 20 kHz and 1 s as a recycle delay. [$Al(NO_3)_3 \cdot 9H_2O$] was used as a secondary reference (0 ppm). X-Ray photoelectron spectroscopy (XPS) spectra of the reduced [Ag/Mg_4Al-LDH] catalyst and the material recovered after reaction use were recorded with a SPECS spectrometer equipped with a Phibos 150 MCD-9 multichannel analyzer, using a non-monochromatic MgK (1253.6 eV) X-ray source. The spectra were recorded with an X-ray power of 100 W, pass energy of 30 eV, and under an operating pressure of 10–9 mbar. The XPS spectra were referenced to C1s peak (284.5 eV), and spectra treatment was performed using the CASA XPS software.

General procedures for materials preparation

Synthesis of [Mg_xAl-LDH] supports.[22e] [Mg_2Al-LDH], [Mg_3Al-LDH], [Mg_4Al-LDH] and [Mg_5Al-LDH] supports were prepared by a co-precipitation method at pH 10 following a known procedure as follows. 200 mL of a x·[0.25 M] (x = 2, 3, 4 or 5) and [0.25 M] aqueous solution of [$Mg(NO_3)_2 \cdot 6H_2O$] (99%) and [$Al(NO_3)_3 \cdot 9H_2O$] (> 98%), respectively, were added dropwise under N_2 to a three-neck round-bottom flask containing 240 mL of [2 M] aqueous solution of Na_2CO_3 (> 99.5%), keeping under agitation at ambient temperature. A [40 wt%] NaOH (97%) aqueous solution was simultaneously added dropwise to keep a constant pH around 10. Then, the obtained slurry was aged at 60 °C for 6 h under stirring, filtered under vacuum and washed (3×100 mL of ultrapure water), and the precipitate was dried under vacuum at 100 °C overnight.

Synthesis of [Ag/Mg_4Al-LDH] material. $AgNO_3$ (≥ 99.0%, 11.8 mg, 0.069 mmol Ag) was added into a 100 mL round-bottom flask and dissolved in 30 mL of ultrapure water. Then, the solution was heated up to 55 °C under stirring and [Mg_4Al-LDH] support (992.5 mg) was added, maintaining the mixture under stirring at 55 °C for 4 h. After this, the solid was filtered under vacuum, washed thoroughly with ultrapure water and dried under vacuum at 100 °C for 2 h. Finally, reduction of the obtained solid under hydrogen flow at 130 °C, during 2 h with a heating ramp of 0.5 °C/min (or 1, 2 and 4 °C/min when indicated), afforded [Ag/Mg_4Al-LDH] material with a 0.5 wt% silver content measured by ICP-AES. For obtaining [Ag/Mg_4Al-LDH] catalyst with 0.25 or 1.5 wt% of silver loading, the amount of silver nitrate was changed accordingly.

General catalytic procedures

General procedure for catalytic studies in the α-benzylation of 2-phenylacetonitrile (1) with benzyl alcohol (2). A 7 mL glass vial containing a stirring bar was sequentially charged with phenylacetonitrile **1** (14.5 μL, 0.125 mmol), benzyl alcohol **2** (39 μL, 0.375 mmol, 3 equiv.), [Ag/Mg_4Al-LDH] (67 mg, 0.5 wt% Ag content, 2.5 mol% Ag), *n*-hexadecane (7.7 mg, 0.03 mmol) as an internal standard, and mesitylene (2 mL) as solvent under nitrogen atmosphere. Afterwards, the reaction vial was capped with a septum and placed into an aluminium block, which was preheated at 140 °C. After 16 h, the reaction vial was cooled down to room temperature and finally, the reaction mixture was diluted with ethyl acetate, centrifuged and the supernatant was analyzed by GC. The evaluation of the other catalysts was performed in the same way only modifying the employed material as catalyst.

General procedure for the synthesis of α-functionalized nitriles and 2-oxindoles through [Ag/Mg_4Al-LDH]-catalyzed α-alkylations using primary alcohols. A 7 mL glass vial containing a stirring bar was sequentially charged with the corresponding nitrile or 2-oxindole (0.125 mmol), alcohol (0.375 or 0.625 mmol, 3 or 5 equiv.), [Ag/Mg_4Al-LDH] (67 or 134 mg, 0.5 wt% Ag content, 2.5 or 5 mol% Ag), *n*-hexadecane (7.7 mg, 0.03 mmol) as an internal standard, and mesitylene (1.5 mL) as solvent under nitrogen atmosphere. Afterwards, the reaction vial was capped with a septum and placed into an aluminium block, which was preheated at 140 °C. After the indicated time (24 or 48 h), the reaction vial was cooled down to room temperature, diluted with ethyl acetate and centrifuged, and the supernatant was analyzed by GC and GC-MS to confirm the progress of the reaction. Then, the crude was filtered to remove the catalyst, washed with ethyl acetate and concentrated under reduced pressure. Finally, the residue was purified by column chromatography using (hexane/AcOEt) mixtures as eluent to afford the desired α-functionalized product.

General procedure for the synthesis of 3-arylquinolin-2(1*H*)-ones via intramolecular [Ag/Mg_4Al-LDH]-catalyzed α-alkylation of *N*-(2-(hydroxymethyl)phenyl)-2-phenylacetamides. A 7 mL glass vial containing a stirring bar was sequentially charged with the corresponding *N*-(2-(hydroxymethyl)phenyl)-2-phenylacetamide (0.125 mmol), [Ag/Mg_4Al-LDH] (134 mg, 0.5 wt% Ag content, 5 mol% Ag) and mesitylene (2 mL) as solvent under air atmosphere. Next, the reaction vial was capped with a septum and placed into an aluminium block, which was preheated at 110 °C. After 24 h, the temperature was raised to 140 °C and the reaction was maintained at this temperature during 6 h, and then, the reaction vial was hot filtered using a filter plate to remove the catalyst. Subsequently, the liquid phase was cooled down in an ice bath and a solid precipitation was observed. The solid was separated by centrifugation, washed with cold mesitylene, hexane and ethyl acetate, and was identified as the desired 3-arylquinolin-2(1*H*)-one.

Supporting Information

The authors have cited additional references within the Supporting Information.[47–62]

Acknowledgements

This work was supported by the SEJI program funded by Generalitat Valenciana (Subvencions Excelencia Juniors Investigadors, grants SEJI/2019/006 and SEJI/2020/013), RETOS I+D+I program from MICINN (PID2019-109656RA-I0/AEI/10.13039/501100011033) and a program from "La Caixa" Foundation (ID 100010434), fellowship code LCF/BQ/PI18/11630023. R. A. and J. R. C.-A. thank to MICINN (Spanish Government) for two Ramón y Cajal contracts (ref. RYC2020-029493-I and RYC-2017-22717). The microscopy service of UPV and the analytical services of ITQ are acknowledge for their help.

Conflict of Interests

The authors declare no conflict of interest.

Data Availability Statement

The data that support the findings of this study are available in the supplementary material of this article.

Keywords: Borrowing hydrogen · C–C coupling · Heterogeneous catalysis · Silver · Layered double hydroxides

[1] a) M. J. Climent, A. Corma, S. Iborra, *ChemSusChem* **2009**, *2*, 500–506; b) L. Liu, A. Corma, *Chem. Rev.* **2018**, *118*, 4981–5079; c) Z. Li, S. Ji, Y. Liu, X. Cao, S. Tian, Y. Chen, Z. Niu, Y. Li, *Chem. Rev.* **2020**, *120*, 623–682; d) F. Zaera, *Chem. Rev.* **2022**, *122*, 8594–8757.

[2] a) G. Guillena, D. J. Ramón, M. Yus, *Angew. Chem. Int. Ed.* **2007**, *46*, 2358–2364; b) M. H. S. A. Hamid, P. A. Slatford, J. M. J. Williams, *Adv. Synth. Catal.* **2007**, *349*, 1555–1575; c) Y. Obora, *ACS Catal.* **2014**, *4*, 3972–3981; d) F. Huang, Z. Liu, Z. Yu, *Angew. Chem. Int. Ed.* **2016**, *55*, 862–875; e) A. Corma, J. Navas, M. J. Sabater, *Chem. Rev.* **2018**, *118*,

1410–1459; f) T. Irrgang, R. Kempe, *Chem. Rev.* **2019**, *119*, 2524–2549; g) B. G. Reed-Berendt, D. E. Latham, M. B. Dambatta, L. C. Morrill, *ACS Cent. Sci.* **2021**, *7*, 570–585; h) K. Sun, H. Shan, G. P. Lu, C. Cai, M. Beller, *Angew. Chem. Int. Ed.* **2021**, *60*, 25188–25202; i) K.-i. Shimizu, *Catal. Sci. Technol.* **2015**, *5*, 1412–1427.

[3] a) D. G. Evans, X. Duan, *Chem. Commun.* **2006**, 485–496 ; b) G. R. Williams, D. O'Hare, *J. Mater. Chem.* **2006**, *16*, 3065–3074; c) J. M. Oh, T. T. Biswick, J. H. Choy, *J. Mater. Chem.* **2009**, *19*, 2553–2563; d) G. Fan, F. Li, D. G. Evans, X. Duan, *Chem. Soc. Rev.* **2014**, *43*, 7040–7066; e) S. Omwoma, W. Chen, R. Tsunashima, Y.-F. Song, *Coord. Chem. Rev.* **2014**, *258–259*, 58–71; f) T. Baskaran, J. Christopher, A. Sakthivel, *RSC Adv.* **2015**, *5*, 98853–98875; g) M. Xu, M. Wei, *Adv. Funct. Mater.* **2018**, *28*, 1–20; h) K. Kaneda, T. Mizugaki, *Green Chem.* **2019**, *21*, 1361–1389.

[4] a) D. P. Debecker, E. M. Gaigneaux, G. Busca, *Chem. Eur. J.* **2009**, *15*, 3920–3935; b) F. L. Theiss, G. A. Ayoko, R. L. Frost, *Appl. Surf. Sci.* **2016**, *383*, 200–213.

[5] a) N. Kurono, T. Ohkuma, *ACS Catal.* **2016**, *6*, 989–1023; b) R. Lopez, C. Palomo, *Angew. Chem. Int. Ed.* **2015**, *54*, 13170–13184.

[6] a) F. F. Fleming, *Nat. Prod. Rep.* **1999**, *16*, 597–606; b) F. F. Fleming, L. Yao, P. C. Ravikumar, L. Funk, B. C. Shook, *J. Med. Chem.* **2010**, *53*, 7902–7917.

[7] a) A. Fensome, R. Bender, J. Cohen, M. A. Collins, V. A. Mackner, L. L. Miller, J. W. Ullrich, R. Winneker, J. Wrobel, P. Zhang, Z. Zhang, Y. Zhu, *Bioorg. Med. Chem. Lett.* **2002**, *12*, 3487–3490; b) J. L. Whatmore, E. Swann, P. Barraja, J. J. Newsome, M. Bunderson, H. D. Beall, J. E. Tooke, C. J. Moody, *Angiogenesis* **2002**, *5*, 45–51; c) S. Peddibhotla, *Curr. Bioact. Compd.* **2009**, *5*, 20–38; d) A. P. Antonchick, C. Gerding-Reimers, M. Catarinella, M. Schuermann, H. Preut, S. Ziegler, D. Rauh, H. Waldmann, *Nat. Chem.* **2010**, *2*, 735–740; e) T. Rodrigues, D. Reker, P. Schneider, G. Schneider, *Nat. Chem.* **2016**, *8*, 531–541; f) Y. M. Khetmalis, M. Shivani, S. Murugesan, K. V. G. Chandra Sekhar, *Biomed. Pharmacother.* **2021**, *141*, 111842–111842.

[8] T. Kagata, S. Saito, H. Shigemori, A. Ohsaki, H. Ishiyama, T. Kubota, J. i. Kobayashi, *J. Nat. Prod.* **2006**, *69*, 1517–1521.

[9] https://organicchemistrydata.org/hansreich/resources/pka/.

[10] a) I. Gruda, *Can. J. Chem.* **1972**, *50*, 18–23; b) A. S. Kende, J. C. Hodges, *Synth. Commun.* **1982**, *12*, 1–10; c) S. Arseniyadis, K. S. Kyler, D. S. Watt, *Addition and substitution reactions of nitrile-stabilized carbanions, Vol. 31*, Wiley, **1984**; d) D. F. Taber, S. Kong, *J. Org. Chem.* **1997**, *62*, 8575–8576; e) F. F. Fleming, W. Liu, S. Ghosh, O. W. Steward, *J. Org. Chem.* **2008**, *73*, 2803–2810; f) B. Volk, J. Barkoczy, E. Hegedus, S. Udvari, I. Gacsalyi, T. Mezei, K. Pallagi, H. Kompagne, G. Levay, A. Egyed, L. G. Harsing Jr., M. Spedding, G. Simig, *J. Med. Chem.* **2008**, *51*, 2522–2532.

[11] For selected examples involving the homogeneously catalyzed BH between nitriles or oxindoles an alcohols see: a) R. Grigg, T. R. B. Mitchell, S. Sutthivaiyakit, N. Tongpenyai, *Tetrahedron Lett.* **1981**, *22*, 4107–4107; b) P. J. Black, G. Cami-Kobeci, M. G. Edwards, P. A. Slatford, M. K. Whittlesey, J. M. J. Williams, *Org. Biomol. Chem.* **2006**, *4*, 116–125; c) T. Jensen, R. Madsen, C. Screening, *J. Org. Chem.* **2009**, *74*, 3990–3992; d) M. L. Buil, M. A. Esteruelas, J. Herrero, S. Izquierdo, I. M. Pastor, M. Yus, *ACS Catal.* **2013**, *3*, 2072–2075; e) M. Peña-López, P. Piehl, S. Elangovan, H. Neumann, M. Beller, *Angew. Chem. Int. Ed.* **2016**, *55*, 14967–14971; f) A. Jana, C. B. Reddy, B. Maji, *ACS Catal.* **2018**, *8*, 9226–9231; g) W. Ma, S. Cui, H. Sun, W. Tang, D. Xue, C. Li, J. Fan, J. Xiao, C. Wang, *Chem. Eur. J.* **2018**, *24*, 13118–13123; h) K. Polidano, B. D. W. Allen, J. M. J. Williams, L. C. Morrill, *ACS Catal.* **2018**, *8*, 6440–6445; i) J. Sklyaruk, J. C. Borghs, O. El-Sepelgy, M. Rueping, *Angew. Chem. Int. Ed.* **2019**, *58*, 775–779; j) P. Chakraborty, N. Garg, E. Manoury, R. Poli, B. Sundararaju, *ACS Catal.* **2020**, *10*, 8023–8031; k) S. Wang, D. Song, F. Shen, R. Chen, Y. Cheng, C. Zhao, Q. Shen, S. Yin, F. Ling, W. Zhong, *Green Chem.* **2022**, *25*, 357–364.

[12] For a metal-free base promoted alfa-alkylation of nitriles with alcohols, see: B. C. Roy, I. A. Ansari, S. A. Samim, S. Kundu, *Chem. Asian J.* **2019**, *14*, 2215–2219.

[13] a) K. Motokura, D. Nishimura, K. Mori, T. Mizugaki, K. Ebitani, K. Kaneda, *J. Am. Chem. Soc.* **2004**, *126*, 5662–5663; b) K. Motokura, N. Fujita, K. Mori, T. Mizugaki, K. Ebitani, K. Jitsukawa, K. Kaneda, *Chem. Eur. J.* **2006**, *12*, 8228–8239.

[14] A. Corma, T. Ródenas, M. J. Sabater, *J. Catal.* **2011**, *279*, 319–327.

[15] F. Bartoccini, M. Retini, G. Piersanti, *Tetrahedron Lett.* **2020**, *61*, 151875–151875.

[16] a) E. Wenkert, N. V. Bringi, *J. Am. Chem. Soc.* **1958**, *80*, 5575–5576; b) B. Volk, T. Mezei, G. Simig, *Synthesis* **2002**, *5*, 595–597.

[17] a) G. Liu, T. Huang, Y. Zhang, X. Liang, Y. Li, H. Li, *Catal. Commun.* **2011**, *12*, 655–659; b) C. Chaudhari, S. M. A. H. Siddiki, K. Kon, A. Tomita, Y. Tai, K.-i. Shimizu, *Catal. Sci. Technol.* **2014**, *4*, 1064–1069; c) A. E. Putra, Y. Oe, T. Ohta, *Eur. J. Org. Chem.* **2015**, *2015*, 7799–7805.

[18] S. Fujita, K. Imagawa, S. Yamaguchi, J. Yamasaki, S. Yamazoe, T. Mizugaki, T. Mitsudome, *Sci. Rep.* **2021**, *11*, 1–10.

[19] a) T. Mitsudome, Y. Mikami, M. Matoba, T. Mizugaki, K. Jitsukawa, K. Kaneda, *Angew. Chem. Int. Ed.* **2012**, *51*, 136–139; b) Y. Xie, P. Hu, T. Bendikov, D. Milstein, *Catal. Sci. Technol.* **2018**, *8*, 2784–2788; c) W. Gong, Q. Wu, G. Jiang, G. Li, *J. Mater. Chem. A* **2019**, *7*, 13449–13454; d) R. Coeck, J. Meeprasert, G. Li, T. Altantzis, S. Bals, E. A. Pidko, D. E. De Vos, *ACS Catal.* **2021**, *11*, 7672–7684.

[20] a) T. Mitsudome, Y. Mikami, H. Funai, T. Mizugaki, K. Jitsukawa, K. Kaneda, *Angew. Chem. Int. Ed.* **2008**, *47*, 138–141; b) K.-i. Shimizu, R. Sato, A. Satsuma, *Angew. Chem. Int. Ed.* **2009**, *48*, 3982–3986; c) K.-i. Shimizu, K. Sugino, K. Sawabe, A. Satsuma, *Chem. Eur. J.* **2009**, *15*, 2341–2351; d) G. V. Mamontov, M. V. Grabchenko, V. I. Sobolev, V. I. Zaikovskii, O. V. Vodyankina, *Appl. Cat. A Gen.* **2016**, *528*, 161–167.

[21] a) M. Lakshmi Kantam, B. M. Choudary, C. Venkat Reddy, K. Koteswara Rao, M. Lakshmi Kantam, B. M. Choudary, K. Koteswara Rao, F. Figueras, *Chem. Commun.* **1998**, 1033–1034; b) M. L. Kantam, A. Ravindra, C. V. Reddy, B. Sreedhar, B. M. Choudary, *Adv. Synth. Catal.* **2006**, *348*, 569–578; c) W. Bing, L. Zheng, S. He, D. Rao, M. Xu, L. Zheng, B. Wang, Y. Wang, M. Wei, *ACS Catal.* **2018**, *8*, 656–664.

[22] a) M. Vucelic, G. D. Moggridge, W. Jones, *J. Phys. Chem.* **1995**, *99*, 8328–8337; b) A. Vaccari, *Catal. Today* **1998**, *41*, 53–71; c) J. Pérez-Ramírez, S. Abelló, N. M. Van Der Pers, *Chem. Eur. J.* **2007**, *13*, 870–878; d) A. Forticaux, L. Dang, H. Liang, S. Jin, *Nano Lett.* **2015**, *15*, 3403–3409; e) G. M. Lari, G. Pastore, C. Mondelli, J. Pérez-Ramírez, *Green Chem.* **2018**, *20*, 148–159.

[23] S. M. Ashekuzzaman, J.-Q. Jiang, *Chem. Eng. J.* **2014**, *246*, 97–105.

[24] a) J. Z. Zhou, Z. P. Xu, S. Qiao, J. Liu, Q. Liu, Y. Xu, J. Zhang, G. Qian, *Appl. Clay Sci.* **2011**, *54*, 196–201; b) W. Wu, Y. Wu, B. Jin, Q. Gu, *ACS Omega* **2019**, *4*, 18159–18166.

[25] K. Shekoohi, F. S. Hosseini, A. H. Haghighi, A. Sahrayian, *MethodsX* **2017**, *4*, 86–94.

[26] R. G. Prado, G. D. Almeida, A. R. de Oliveira, P. M. T. G. de Souza, C. C. Cardoso, V. R. L. Constantino, F. G. Pinto, J. Tronto, V. M. D. Pasa, *Energy Fuels* **2016**, *30*, 6662–6670.

[27] a) S. Abelló, F. Medina, D. Tichit, J. Pérez-Ramírez, J. C. Groen, J. E. Sueiras, P. Salagre, Y. Cesteros, *Chem. Eur. J.* **2005**, *11*, 728–739; b) J. S. Valente, H. Pfeiffer, E. Lima, J. Prince, J. Flores, *J. Catal.* **2011**, *279*, 196–204; c) Z. Ren, Y. Yang, S. Wang, X. Li, H. Feng, L. Wang, Y. Li, X. Zhang, M. Wei, *Appl. Cat. B Environ.* **2021**, *295*, 120290–120290.

[28] K. K. Rao, M. Gravelle, J. S. Valente, F. Figueras, *J. Catal.* **1998**, *173*, 115–121.

[29] R. J. Chimentão, S. Abelló, F. Medina, J. Llorca, J. E. Sueiras, Y. Cesteros, P. Salagre, *J. Catal.* **2007**, *252*, 249–257.

[30] a) N. D. Hutson, B. A. Reisner, R. T. Yang, B. H. Toby, *Chem. Mater.* **2000**, *12*, 3020–3031; b) A. M. Ferraria, A. P. Carapeto, A. M. Botelho do Rego, *Vacuum* **2012**, *86*, 1988–1991; c) A. V. Bukhtiyarov, A. Y. Stakheev, A. I. Mytareva, I. P. Prosvirin, V. I. Bukhtiyarov, *Russ. Chem. Bull.* **2015**, *64*, 2780–2785.

[31] a) G. Mitrikas, C. C. Trapalis, N. Boukos, V. Psyharis, L. Astrakas, G. Kordas, *J. Non-Cryst. Solids* **1998**, *224*, 17–22; b) N. Salam, S. K. Kundu, R. A. Molla, P. Mondal, A. Bhaumik, S. M. Islam, *RSC Adv.* **2014**, *4*, 47593–47604; c) R. A. Molla, K. Ghosh, B. Banerjee, M. A. Iqubal, S. K. Kundu, S. M. Islam, A. Bhaumik, *J. Colloid Interface Sci.* **2016**, *477*, 220–229.

[32] a) K. A. Bethke, H. H. Kung, *J. Catal.* **1997**, *172*, 93–102; b) A. Keshavaraja, X. She, M. Flytzani-Stephanopoulos, *Appl. Cat. B Environ.* **2000**, *27*, L1–L9; c) X. She, M. Flytzani-Stephanopoulos, *J. Catal.* **2006**, *237*, 79–93; d) N. Popovych, P. Kyriienko, S. Soloviev, R. Baran, Y. Millot, S. Dzwigaj, *Phys. Chem. Chem. Phys.* **2016**, *18*, 29458–29465; e) I. López-Hernández, C. García, V. Truttmann, S. Pollitt, N. Barrabés, G. Rupprechter, F. Rey, A. E. Palomares, *Catal. Today* **2020**, *345*, 22–26.

[33] K. Paudel, S. Xu, K. Ding, *J. Org. Chem.* **2020**, *85*, 14980–14988.

[34] a) J. S. Valente, H. Pfeiffer, E. Lima, J. Prince, J. Flores, *J. Catal.* **2011**, *279*, 196–204; b) C. Cuautli, J. S. Valente, J. C. Conesa, M. V. Ganduglia-Pirovano, J. Ireta, *J. Phys. Chem. C* **2019**, *123*, 8777–8784.

[35] K.-i. Shimizu, K. Sugino, K. Sawabe, A. Satsuma, *Chem. Eur. J.* **2009**, *15*, 2341–2351.

[36] a) K.-i. Shimizu, Y. Miyamoto, A. Satsuma, *J. Catal.* **2010**, *270*, 86–94; b) J. Zou, X. Duan, X. Liu, L. Huang, X. Liu, J. Zuo, W. Jiao, H. Lin, L. Ye, Y. Yuan, *Chem. Eng. J.* **2023**, *454*, 140110.

[37] K. Ebitani, K. Motokura, K. Mori, T. Mizugaki, K. Kaneda, *J. Org. Chem.* **2006**, *71*, 5440–5447.

[38] a) Y. Iuchi, Y. Obora, Y. Ishii, *J. Am. Chem. Soc.* **2010**, *132*, 2536–2537; b) L. Guo, X. Ma, H. Fang, X. Jia, Z. Huang, *Angew. Chem. Int. Ed.* **2015**, *54*, 4023–4027; c) N. Deibl, R. Kempe, *J. Am. Chem. Soc.* **2016**, *138*, 10786–10789; d) S. Chakraborty, P. Daw, Y. Ben David, D. Milstein, *ACS Catal.* **2018**, *8*, 10300–10305.
[39] H. Iguchi, N. Katayama, T. Suzuki, T. Fujihara, Y. Jing, T. Toyao, Z. Maeno, K.-i. Shimizu, Y. Obora, *Chem. Commun.* **2022**, *58*, 11851–11854.
[40] a) S. Heeb, M. P. Fletcher, S. R. Chhabra, S. P. Diggle, P. Williams, M. Cámara, *FEMS Microbiol. Rev.* **2011**, *35*, 247–274; b) C. B. M. Poulie, L. Bunch, *ChemMedChem* **2013**, *8*, 205–215; c) L. B. Rao, C. Sreenivasulu, D. R. Kishore, G. Satyanarayana, *Tetrahedron* **2022**, *127*, 133093.
[41] a) K. K. Park, J. Y. Jung, *Heterocycles* **2005**, *65*, 2095–2105; b) S.-Y. Han, J. W. Choi, J. Yang, C. H. Chae, J. Lee, H. Jung, K. Lee, J. D. Ha, H. R. Kim, S. Y. Cho, *Bioorg. Med. Chem. Lett.* **2012**, *22*, 2837–2842.
[42] a) G. Uray, K. S. Niederreiter, F. Belaj, W. M. F. Fabian, *Helv. Chim. Acta* **1999**, *82*, 1408–1417; b) X. Liu, X. Xin, D. Xiang, R. Zhang, S. Kumar, F. Zhou, D. Dong, *Org. Biomol. Chem.* **2012**, *10*, 5643–5646; c) X. Wu, W. Li, *J. Heterocycl. Chem.* **2022**, *59*, 1445–1490.
[43] a) B. Joseph, F. Darro, A. Béhard, B. Lesur, F. Collignon, C. Decaestecker, A. Frydman, G. Guillaumet, R. Kiss, *J. Med. Chem.* **2002**, *45*, 2543–2555; b) Y. Zhang, Y. Fang, H. Liang, H. Wang, K. Hu, X. Liu, X. Yi, Y. Peng, *Bioorg. Med. Chem. Lett.* **2013**, *23*, 107–111.
[44] a) M. Arisawa, A. Nishida, M. Nakagawa, *J. Organomet. Chem.* **2006**, *691*, 5109–5121; b) Z. Zhang, R. Li, *Chem. Heterocycl. Compd.* **2020**, *56*, 509–511.
[45] M. E. Diener, A. J. Metrano, S. Kusano, S. J. Miller, *J. Am. Chem. Soc.* **2015**, *137*, 12369–12377.
[46] G. Chidambaram, M. David, *Science* **2013**, *341*, 1229712–1229712.
[47] A. Tsuji, K. T. V. Rao, S. Nishimura, A. Takagaki, K. Ebitani, *ChemSusChem* **2011**, *4*, 542–548.
[48] F. Li, X. Zou, N. Wang, *Adv. Synth. Catal.* **2015**, *357*, 1405–1415.
[49] S. Huang, X. Hong, Y. Sun, H. Z. Cui, Q. Zhou, Y. J. Lin, X. F. Hou, *Appl. Organomet. Chem.* **2020**, *34*, 1–13.
[50] S. Bera, A. Bera, D. Banerjee, *Chem. Commun.* **2020**, *56*, 6850–6853.
[51] Z.-H. Zhu, Y. Li, Y.-B. Wang, Z.-G. Lan, X. Zhu, X.-Q. Hao, M.-P. Song, *Organometallics* **2019**, *38*, 2156–2166.
[52] A. Singh, M. Findlater, *Organometallics* **2022**, *41*, 3145–3151.
[53] C. Löfberg, R. Grigg, M. A. Whittaker, A. Keep, A. Derrick, *J. Org. Chem.* **2006**, *71*, 8023–8027.
[54] M. H. Ku, H. K. Oh, S. Ko, *Bull. Korean Chem. Soc.* **2007**, *28*, 1217–1220.
[55] J. Li, Y. Liu, W. Tang, D. Xue, C. Li, J. Xiao, C. Wang, *Chem. Eur. J.* **2017**, *23*, 14445–14449.
[56] J. Xiao, F. Li, T. Zhong, X. Wu, F. Guo, Q. Li, Z. L. Tang, *Tetrahedron* **2020**, *76*, 131621–131621.
[57] R. Grigg, S. Whitney, V. Sridharan, A. Keep, A. Derrick, *Tetrahedron* **2009**, *65*, 4375–4383.
[58] J. Schmid, T. Junge, J. Lang, W. Frey, R. Peters, *Angew. Chem. Int. Ed.* **2019**, *58*, 5447–5451.
[59] H. Shen, Y. Du, J. Kan, W. Su, *Org. Biomol. Chem.* **2022**, *20*, 3589–3597.
[60] Y. Liu, Y. Mao, Y. Hu, J. Gui, L. Wang, W. Wang, S. Zhang, *Adv. Synth. Catal.* **2019**, *361*, 1554–1558.
[61] Y. Liu, X. Qi, X.-F. Wu, *J. Org. Chem.* **2021**, *86*, 13824–13832.
[62] A. Charoenpol, J. Meesin, O. Khaikate, V. Reutrakul, M. Pohmakotr, P. Leowanawat, D. Soorukram, C. Kuhakarn, *Org. Biomol. Chem.* **2018**, *16*, 7050–7054.

Manuscript received: June 8, 2023
Revised manuscript received: July 24, 2023
Accepted manuscript online: July 24, 2023
Version of record online: September 6, 2023